

Supporting Information

Synthesis, Structures, and Magnetic Properties of a Series of New Heterometallic Hexanuclear Co_2Ln_4 ($\text{Ln} = \text{Eu}, \text{Gd}, \text{Tb}$ and Dy) Clusters

Chong-Bin Tian,^a Da-Qiang Yuan^a, Yun-Hu Han^{a, b} Zhi-Hua Li^a, Ping Lin^a and Shao-Wu Du^{*a}

^a State Key Laboratory of Structure Chemistry, Fujian Institute of Research on the Structure of Matter, Chinese Academy of Sciences. Fujian, Fuzhou 350002, P. R. China.

^b Graduate University of Chinese Academy of Sciences, Beijing 100039, P. R. China.
E-mail: swdu@fjirsm.ac.cn

Table S1. Selected bond lengths (Å) and angles (°) of **1–4**

	1 ($\text{Ln} = \text{Eu}$)	2 ($\text{Ln} = \text{Gd}$)	3 ($\text{Ln} = \text{Tb}$)	4 ($\text{Ln} = \text{Dy}$)
Co(1)–N(1)	1.868 (5)	1.866 (5)	1.880 (7)	1.874 (6)
Co(1)–O(3)	1.885 (4)	1.885 (5)	1.877 (6)	1.886 (5)
Co(1)–O(1)	1.894 (4)	1.905 (4)	1.897 (6)	1.910 (5)
Co(1)–O(7)	1.910 (4)	1.920 (4)	1.916 (5)	1.918 (4)
Co(1)–O(6)	1.919 (4)	1.924 (4)	1.911 (5)	1.912 (4)
Co(1)–N(3)	1.944 (5)	1.943 (5)	1.944 (7)	1.942 (5)
Ln(1)–O(8)	2.378 (4)	2.355 (4)	2.342 (6)	2.329 (4)
Ln(1)–O(4)	2.371 (4)	2.362 (4)	2.335 (5)	2.336 (4)
Ln(1)–O(12)	2.397 (4)	2.384 (4)	2.372 (5)	2.360 (4)
Ln(1)–O(7)	2.408 (4)	2.403 (4)	2.380 (5)	2.369 (4)
Ln(1)–O(12) [#]	2.415 (4)	2.402 (3)	2.395 (5)	2.378 (4)
Ln(1)–O(1)	2.456 (4)	2.440 (4)	2.430 (5)	2.406 (4)
Ln(1)–N(2)	2.530 (5)	2.519 (5)	2.493 (6)	2.493 (5)
Ln(1)–O(6)	2.609 (4)	2.610 (4)	2.611 (5)	2.604 (5)
Ln(1)–O(2)	2.789 (4)	2.820 (4)	2.820 (6)	2.856 (4)
Ln(2)–O(12)	2.384 (4)	2.387 (4)	2.355 (5)	2.352 (4)
Ln(2)–O(9) [#]	2.419 (4)	2.411 (4)	2.389 (6)	2.373 (4)
Ln(2)–O(11)	2.439 (5)	2.416 (5)	2.397 (7)	2.396 (6)
Ln(2)–O(6)	2.456 (4)	2.445 (4)	2.417 (5)	2.401 (4)
Ln(2)–O(3)	2.466 (4)	2.476 (4)	2.453 (5)	2.454 (4)
Ln(2)–O(4) [#]	2.491 (4)	2.470 (4)	2.453 (5)	2.450 (4)
Ln(2)–O(5) [#]	2.497 (4)	2.484 (4)	2.471 (6)	2.450 (4)
Ln(2)–O(10)	2.500 (5)	2.495 (5)	2.499 (6)	2.494 (5)
Ln(2)–O(7)	2.525 (4)	2.527 (4)	2.510 (5)	2.513 (4)
Co(1)…Ln(1)	3.1885 (14)	3.1816 (11)	3.1648 (15)	3.1595 (11)
Co(1)…Ln(2)	3.1683 (14)	3.1649 (12)	3.1484 (16)	3.1415 (10)
Ln(1)…Ln(2)	3.7785 (17)	3.7663 (12)	3.7346 (17)	3.7235 (9)
Ln(1)…Ln(2) [#]	3.8285 (17)	3.8187 (12)	3.7997 (17)	3.7886 (9)

Co(1)–O(1)–	93.38 (15)	93.42 (15)	93.2 (2)	93.40 (16)
Co(1)–O3–Ln2	92.49 (16)	92.02 (17)	92.3 (2)	91.81 (18)
Ln(1)–O(4)–	103.87 (14)	104.39 (14)	105.00 (18)	104.65 (14)
Co(1)–O(6)–	88.14 (14)	87.85 (15)	87.4 (2)	87.39 (16)
Co(1)–O(6)–	91.97 (15)	92.05 (15)	92.6 (2)	92.80 (16)
Ln(2)–O(6)–	96.45 (13)	96.27 (13)	95.85 (17)	96.07 (14)
Co(1)–O(7)–	94.48 (14)	94.21 (14)	94.29 (19)	94.35 (15)
Co(1)–O(7)–	90.09 (14)	89.66 (15)	89.6 (2)	89.25 (17)
Ln(1)–O(7)–	99.94 (13)	99.60 (12)	99.56 (17)	99.35 (14)
Ln(1)–O(12)–	111.99 (14)	112.28 (14)	111.6 (2)	111.78 (16)
Ln(2)–O(12)–	104.45 (14)	104.21 (13)	104.37 (18)	104.41 (14)
Ln(2)–O(12)–	105.85 (14)	105.79 (13)	106.24 (19)	106.43 (14)

Symmetric code: [#] 1 – x , – y , – z .

Thermal stability of complexes **1–3**.

From 40 to 230 °C, The TGA curves of **1–3** show a weight loss of 1.5, 1.5 and 1.54%, respectively, which can be attributed to the loss of two lattice water molecules (calcd = 1.62, 1.61 and 1.60%, respectively). And then, they begin to decompose due to the collapse of organic ligands (Fig. S2). The high thermal stability of **1–3** were further confirmed by the temperature resolved XRD patterns, which were performed after calcination of the samples at elevated temperature in the range of 100–240 °C (Fig. S2).

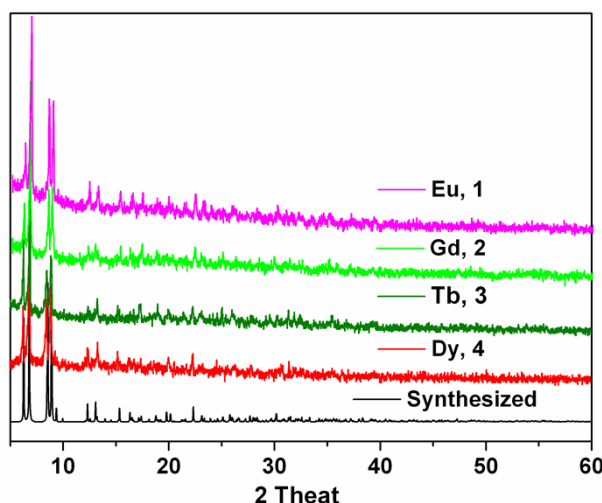


Fig. S1 Experimental and simulated PXRD diagrams of **1–4** at room temperature.

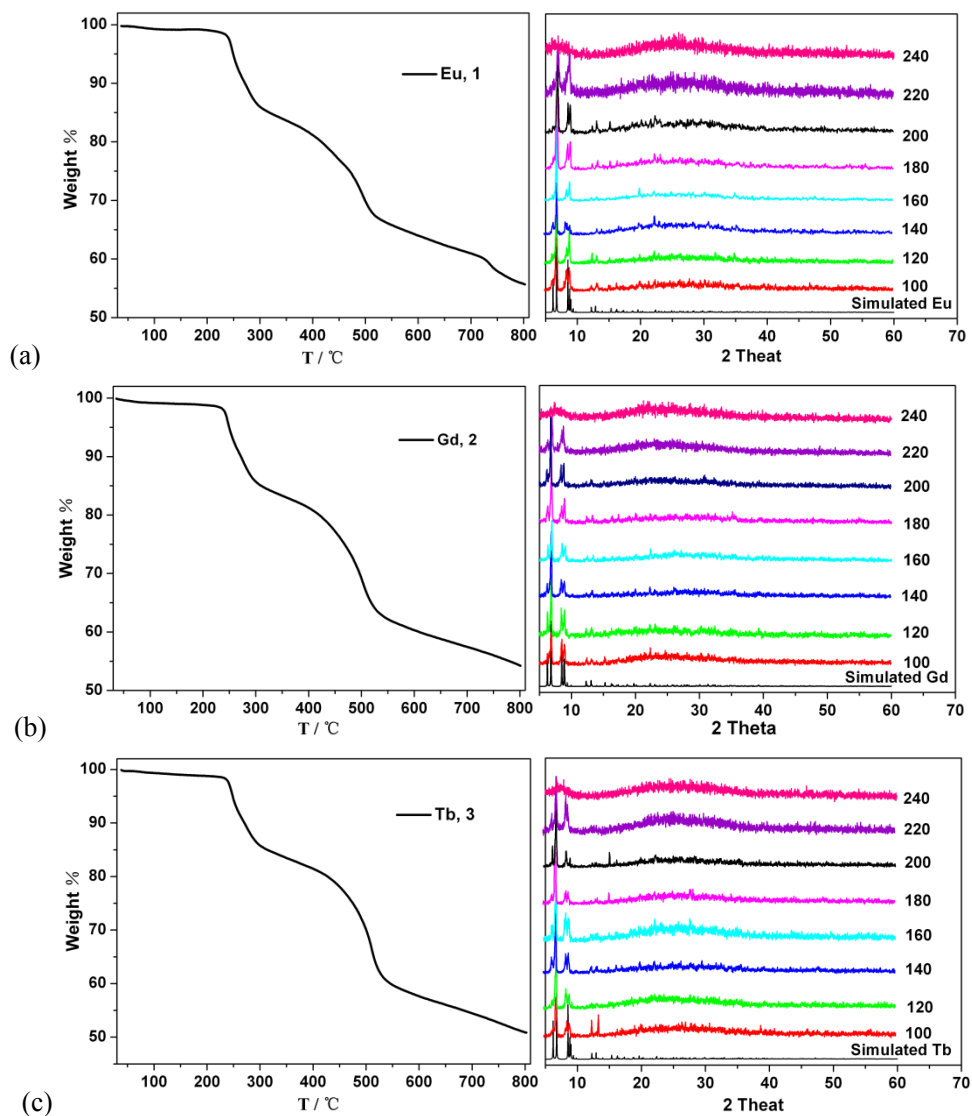


Fig. S2 The TGA and VT XRD curves of compounds **1** (a), **2** (b) and **3** (c).

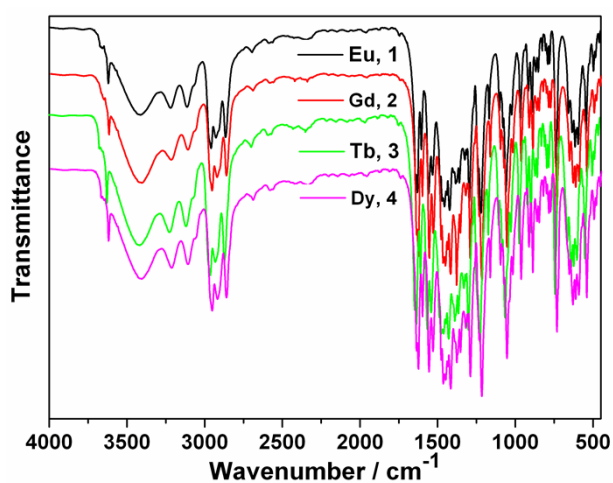


Fig. S3 IR spectra of **1**–**4**.

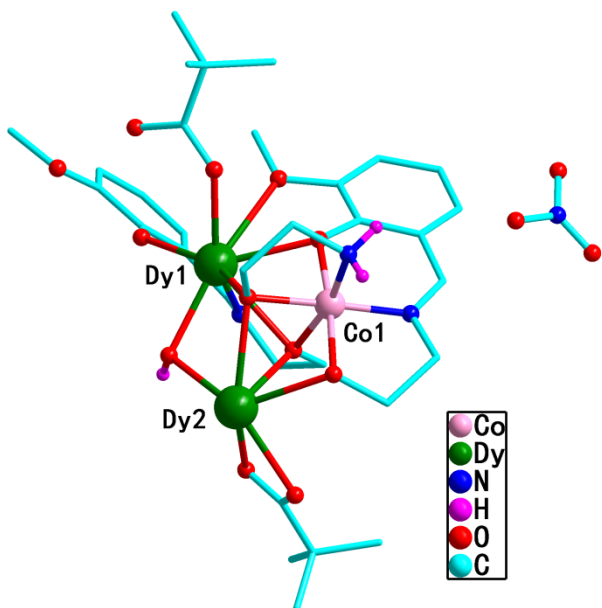


Fig. S4 The asymmetric unit of **4**.

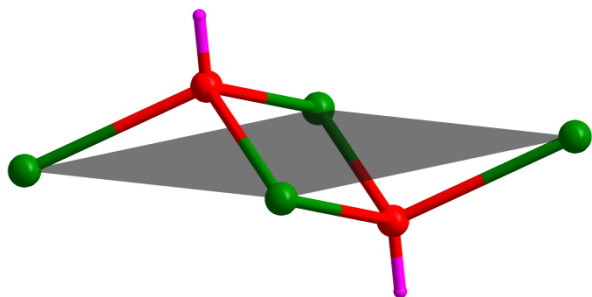


Fig. S5 The planar Dy_4Co_2 core structure of **4**.

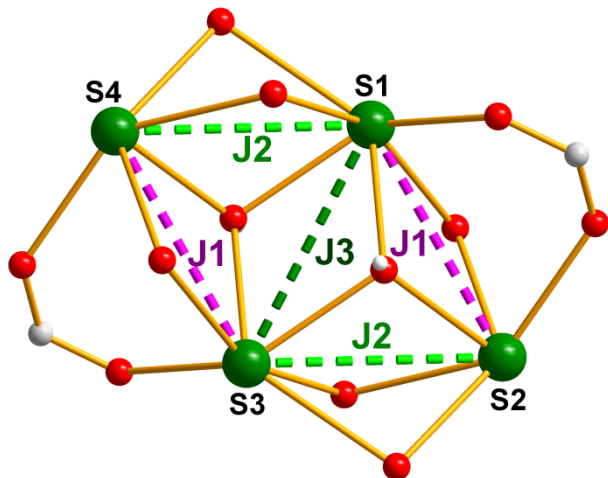


Fig. S6 The three- J exchange mode used for fitting compound **2**. The $\mu_3\text{-OH}$ bridge can be regarded as three $\mu_2\text{-O}$ bridges. Thus, the bridges between Gd^{III} ions in **2** can be divided into three types. Type I: two $\mu_2\text{-O}$ bridges (J_3), type II: three $\mu_2\text{-O}$ bridges (J_2), type III: two $\mu_2\text{-O}$ and one *syn-syn* carboxylate bridges (J_1).

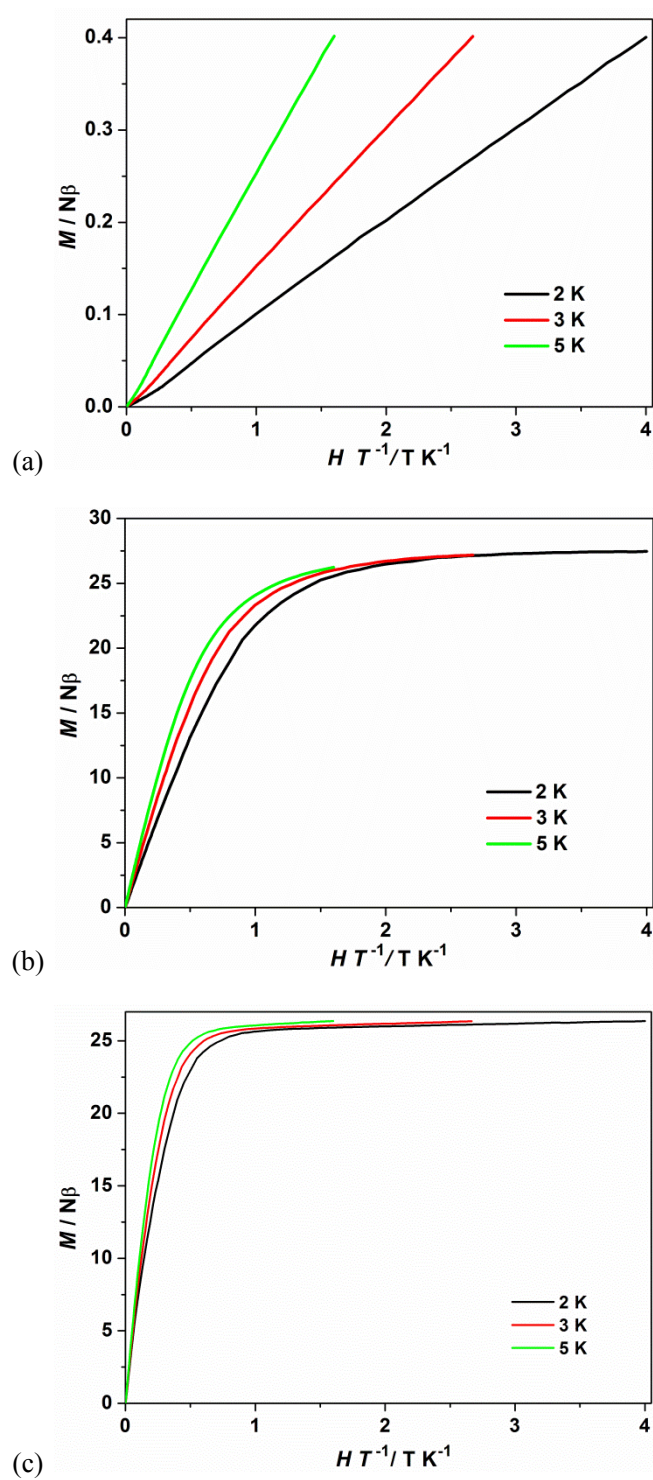


Fig. S7 Plots of M vs. H / T for **1** (a), **2** (b) and **3** (c) at 2, 3 and 5 K.

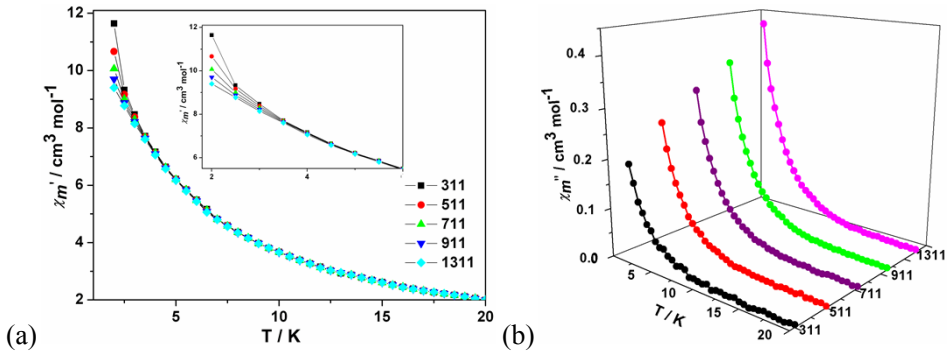


Fig. S8 Temperature dependence of χ_m' (a) and χ_m'' (b) in **4** at various frequencies in $H_{dc} = 0$ Oe.

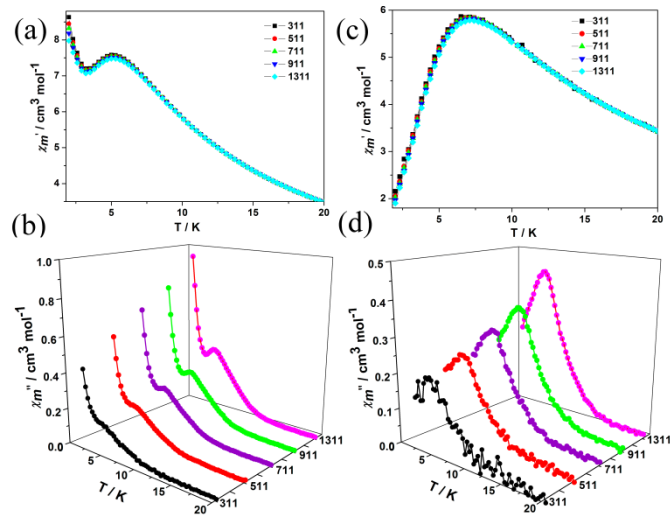


Fig. S9 Temperature dependence of ac susceptibilities in **4** at various frequencies in $H_{dc} = 5000$ Oe ((a) and (b)), $H_{dc} = 8000$ Oe ((c) and (d)).

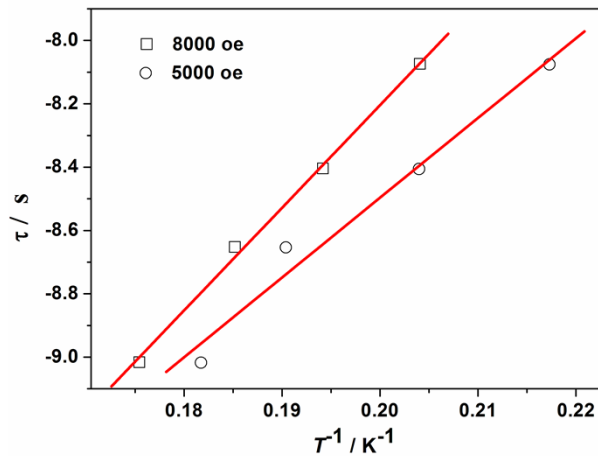


Fig. S10 Magnetization relaxation time $\ln \tau$ vs T^{-1} for **4** under different dc field. The red line is the best fit using the Arrhenius law.

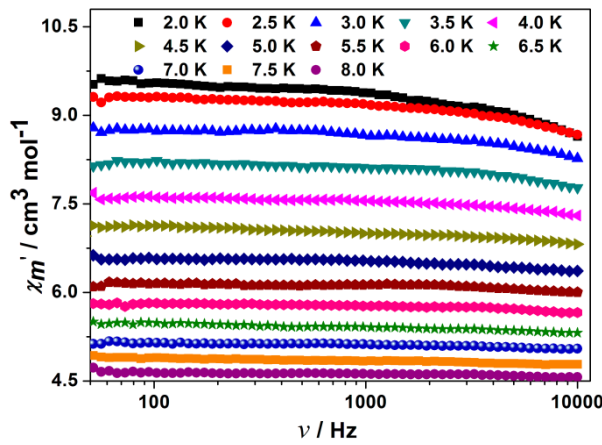


Fig. S11 Frequency dependency in zero dc field of in-phase (χ_m') ac susceptibility component at different temperatures for **4**.

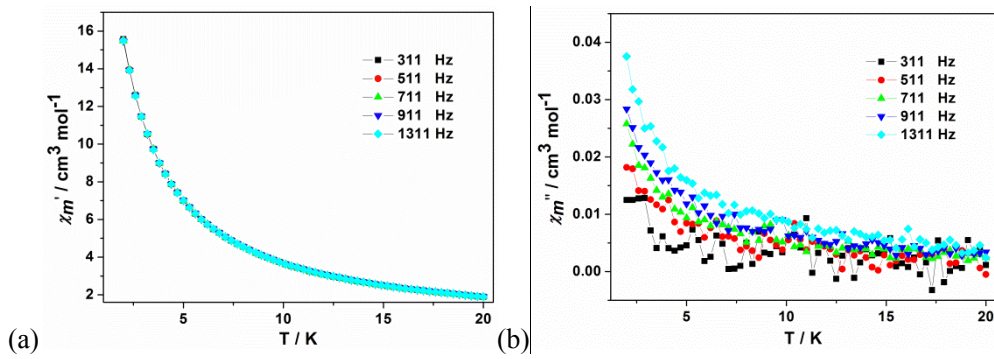


Fig. S12 Temperature dependence of χ_m' (a) and χ_m'' (b) in **3** at various frequencies in $H_{dc} = 0$ Oe.